Supplementary material for : Impact of precessing vortex core dynamics on the thermoacoustic instabilities in a swirl stabilized combustor

Ashwini Karmarkar[1] Saarthak Gupta[2] Isaac Boxx[3] Santosh Hemchandra[2] and Jacqueline O'Connor[1]†,

[1]Department of Mechanical Engineering, Pennsylvania State University, University Park, PA
[2]Department of Aerospace Engineering, Indian Institute of Science, Bengaluru, India
[3]DLR - German Aerospace Center, Stuttgart, Germany

1. Network analysis

1.1. *Structure of interconnections between critical flow regions*

The goal of the discussion in this section is to identify interconnections between the various critical regions in the flow revealed by complex network analysis. This analysis is implemented as follows. We first delete nodes with high closeness centrality in a selected critical region of the flow from the network. Next, the closeness centrality is recomputed on the resulting reduced network and visualized in physical space. The magnitude of the change in closeness centrality in the critical regions retained in the network then quantifies the extent of connectedness between the deleted region and those retained.

As an example of this analysis and its results, the weighted closeness centrality measure for the non-reacting, air split 0.3 case is shown in Fig. 1a. The solid black line is the $u_z = 0$ contour that identifies the extent the vortex breakdown bubble (VBB). The region of high centrality at the upstream end ($z < 10$ mm) of the bubble is identified as the wavemaker region of the PVC oscillation. Oscillations in the shear layer downstream of the wavemaker also have high levels of closeness centrality. Figure 1a shows another region at the downstream end ($z > 15$ mm) of the bubble, which is composed of nodes with large centrality values. Using the technique of selective deletion of nodes described above, we clarify the relationship between this downstream critical region and the other two critical regions located further upstream in the flow. Note first, from Figure 7 in the paper, it is evident that as the air split is increased, the value of the centrality measure in the downstream critical region drops significantly, whereas the value of the centrality measure in the wavemaker region does not change. This suggests that the nodes in this region of the flow become locally less connected with the rest of the network with increasing air split.

We first delete nodes in the PVC wavemaker critical region by setting the correlation coefficient value to zero at nodes with a weighted closeness centrality measure greater than 0.7. Figure 1b shows the spatial distribution of closeness centrality computed for this case. Note that the spatial structure and the value of the centrality measure in the downstream region is unchanged, while some small changes are observed in the

† Email address for correspondence: jxo22@psu.edu

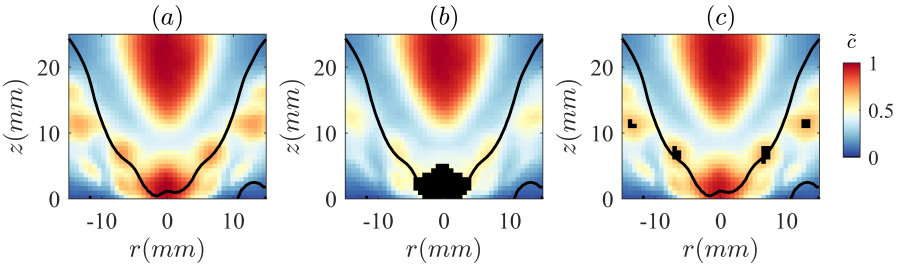

FIGURE 1. Weighted closeness centrality measure from the complex network analysis computed for the radial velocity component for (a) all nodes, (b) with the PVC wavemaker nodes deleted, and (c) with the shear layer nodes deleted.

critical regions in the shear layers. This change shows that the downstream central region is not connected with the wavemaker critical region. Next, we delete nodes using the same criterion in the shear layer critical regions alone; the spatial distribution of closeness centrality for this case is shown in Fig. 1c. Again, the centrality values in the PVC wavemaker critical region marginally reduce while leaving the downstream region unchanged, showing that the downstream critical region is not connected with the shear layer critical regions. Also, since the modal energy spectra from SPOD – see Fig. 5 in the paper – do not show any narrowband oscillations other than the PVC mode, we conclude that the downstream critical region corresponds to correlation due to turbulence and does not constitute the wavemaker region of the PVC mode.

1.2. *Complex network analysis of the air split 0.3 reacting flow case*

Figure 13 in the paper shows the closeness centrality measure for the reacting cases. The centrality measure for the air split 0.3 case has a significantly different structure than the centrality measure for the other air split cases. Figure 12b in the paper shows that for air split < 0.3, TA mode 1 is the only dominant mode, and for the cases with air split > 0.3, the PVC mode governs the dynamics of the flow field. For the air split 0.3 case, Fig. 12b shows that the unsteady flow field is governed by both TA mode 1 and the PVC mode, as they have similar modal amplitudes. Network analysis of this case thus results in a centrality measure driven by both PVC and TA mode 1.

To identify the critical regions corresponding to the PVC and TA modes, we construct reduced flow fields by selectively eliminating contributions from the PVC and the TA mode using a frequency-time decomposition of the unsteady flow field. These types of modal decomposition methods have been developed recently in the past by Mendez *et al.* (2019), Yin & Stöhr (2020), and Gupta *et al.* (2021) in connection with understanding non-stationary flow behavior in a spectrally-selective manner. We apply the wavelet POD method (WPOD) described in detail in Gupta *et al.* (2021) in this section to construct reduced flow fields.

Following Gupta *et al.* (2021), a continuous wavelet transform (CWT) using the bump wavelet is applied on the raw velocity field time series data, $\boldsymbol{q}(x, y, t) = [u_r, u_\theta, u_z]^T$, at each of the PIV grid points. Then, we set all wavelet coefficients at each grid point that lie outside a frequency band of width $\Delta_f = 60$ Hz centered at the frequency of the TA mode 1 (580 Hz) to zero. Note that this center frequency corresponds to the TA mode 1 frequency obtained from SPOD analysis for the air split 0.3 case (refer to Fig. 11 in the paper). Next, we invert the transform at all points that yields wavelet

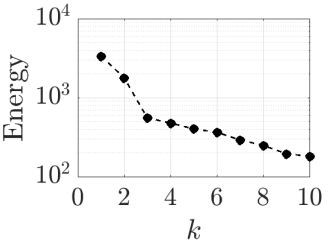

FIGURE 2. Modal energy spectra of the POD modes of the wavelet filtered velocity fields centered at the TA mode 1 ($\tilde{\boldsymbol{q}}_{\boldsymbol{TA}}$) frequency .

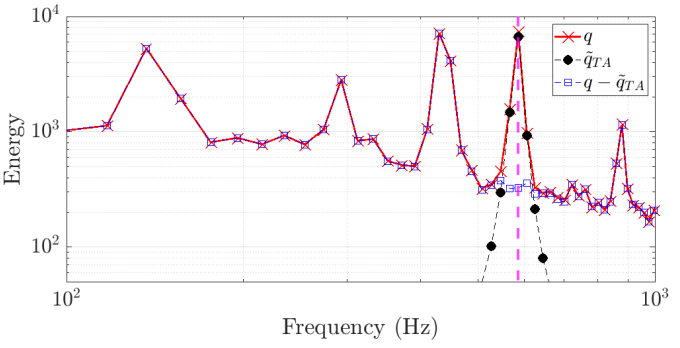

FIGURE 3. Modal energy spectra of velocity fields obtained from spectral POD for raw data, $\boldsymbol{q}$ (solid line with red crosses), wavelet filtered data, $\tilde{\boldsymbol{q}}_{\boldsymbol{TA}}$ (dashed line with black filled circles), and the velocity data with TA mode eliminated, $\boldsymbol{q} - \tilde{\boldsymbol{q}}_{\boldsymbol{TA}}$ (dashed line with blue squares).

filtered snapshots, $\tilde{\boldsymbol{q}}_{\boldsymbol{TA}}(x, y, t)$, which is comprised of spectral content from the raw data only in the vicinity of the TA mode 1 frequency alone. Next, $\tilde{\boldsymbol{q}}_{\boldsymbol{TA}}(x, y, t)$ is decomposed using proper orthogonal decomposition (POD) in terms of spatial modes $\tilde{\phi}_k(x, y)$ and the temporal variations $\tilde{a}_k(t)$ associated with each mode as follows,

$$\tilde{\boldsymbol{q}}_{\boldsymbol{TA}}(x, y, t) = \sum_{k=1}^{N} \sigma_k \tilde{a}_k(t) \tilde{\phi}_k(x, y) \tag{1.1}$$

where N is the number of flow field snapshots, $\hat{\phi}_k$ are mutually orthogonal spatial modes referred to as wavelet-POD (WPOD) modes, $a_k(t)$ determined the contribution of each of the WPOD modes to $\tilde{\boldsymbol{q}}_{\boldsymbol{TA}}$ at each time instant, and σ_k^2 is the contribution from the k^{th} WPOD mode to the overall energy of $\tilde{\boldsymbol{q}}_{\boldsymbol{TA}}$. We then truncate the series in Eq. 1.1 to include contributions from only the most energetic modes. The reduced time series signal with the TA mode 1 eliminated is then computed as $\boldsymbol{q} - \tilde{\boldsymbol{q}}_{\boldsymbol{TA}}$. The same process is applied to construct the reduced field with the PVC mode eliminated.

Figure 2 shows the variation of σ_k for the first 10 modes of the $\tilde{\boldsymbol{q}}_{\boldsymbol{TA}}(x, y, t)$ field. From Fig. 2, it is evident that the first two WPOD modes dominate the overall energy of $\tilde{\boldsymbol{q}}_{\boldsymbol{TA}}$. Therefore, we use the first two modes to reconstruct the flow field by setting $N = 2$ in Eq. 1.1. Figure 3 shows the comparison of the modal energy for the most energetic mode obtained from spectral POD of the time series of the raw data, WPOD reconstructed TA mode 1, and the reduced time series. It is clear that the TA mode 1 has been eliminated in the reduced time series while retaining the background turbulence in its frequency band.

We then compute the centrality measure for the radial velocity component of the flow

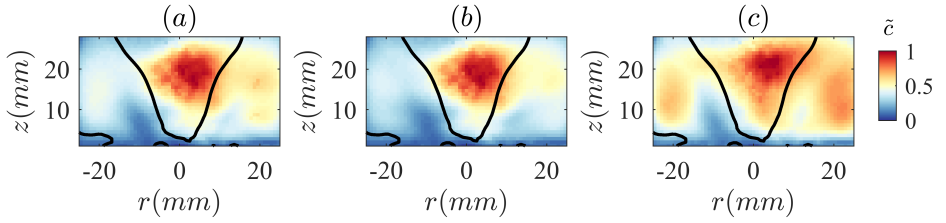

FIGURE 4. Weighted closeness centrality measure computed for the radial velocity component for the (a) raw data $\boldsymbol{q}$, (b) $(\boldsymbol{q} - \tilde{\boldsymbol{q}}_{\boldsymbol{TA}})$, and (c) $(\boldsymbol{q} - \tilde{\boldsymbol{q}}_{\boldsymbol{PVC}})$ for the reacting case at air split = 0.3 case.

fields $(\boldsymbol{q} - \tilde{\boldsymbol{q}}_{\boldsymbol{TA}})$ and $(\boldsymbol{q} - \tilde{\boldsymbol{q}}_{\boldsymbol{PVC}})$. Figures 4a-c show the spatial variations of closeness centrality for the raw time series and the reduced time series without TA mode 1 and PVC contributions, respectively. Note that the spatial distribution of centrality for both reduced fields show a region of strong centrality on the flow centerline at $z \sim 20\ mm$. Additional regions of high centrality are observed in regions directly downstream of the outer nozzle flow regions for the the $(\boldsymbol{q} - \tilde{\boldsymbol{q}}_{\boldsymbol{PVC}})$ case in Fig. 4c. Comparing results in Figs. 4a and b shows that the wavemaker of the PVC-only reduced data in Fig. 4b corresponds closely with the critical region observed in the the raw data. Therefore, because both the PVC and TA mode 1 critical regions on the flow centerline are spatially co-located, the combined effect is region of large centrality in this location as Fig. 4a shows. These results also suggest that the wavemaker for the PVC for the air split 0.3 case alone is somewhat further downstream of the leading edge of the breakdown bubble, possibly due to the lower mass flow rate through the central nozzle when compared to the outer nozzle.

2. Theoretical Formulation

We formulate an asymptotic solution to the variable-density, low Mach number Navier-Stokes equations to gain insight into the underlying mechanisms that determine the coherent flow oscillation behavior of weakly forced, nominally axisymmetric flows that are otherwise self-excited. This analysis extends the weakly nonlinear analysis of Manoharan *et al.* (2020) that analyses self-excited PVC oscillations in a high-Re, variable-S jet. That analysis shows that PVC oscillations are a result of a linear hydrodynamic mode of the jet that becomes marginally stable at a critical swirl number S_c, corresponding to the onset of bubble type vortex breakdown. The velocity fluctuations induced by this mode cause a limit cycle oscillation in the flow characterised by the precession of the vortex breakdown bubble about the flow axis. The value of S_c depends on when the time-averaged flow field can sustain standing waves in a given geometry as suggested by prior studies of vortex breakdown (Benjamin 1962).

The present analysis is motivated by acoustic forcing on the flow induced by thermoacoustic oscillations that are much smaller in amplitude when compared to hydrodynamic response that they introduce. The spectral POD analysis of the experimental data suggests that acoustic forcing from the first thermoacoustic mode excites an axisymmetric *hydrodynamic* response at a fixed frequency. The spectral POD results also show that the amplitude of axisymmetric flow oscillations are strong in the flame region and smaller in regions away from the flame. This suggests that the thermoacoustic pressure oscillation imposes a weak forcing on the time-averaged flow, where 'weak' implies that the amplitude of the *hydrodynamic* response is much larger than that of the imposed

acoustic forcing. Following Manoharan *et al.* (2020), we derive an asymptotic solution for the flow state at a given S assuming a small departure from S_c as follows,

$$S = S_c + \epsilon^2 \Delta_s \tag{2.1}$$

where ϵ is a small number and $\Delta_s \sim O(1)$. Note that this means that the amplitude of the self-excited hydrodynamic oscillation is $O(\epsilon)$. The governing equations are the nonlinear, variable density Navier-Stokes (NS) equations in the low Mach number limit, formulated in a cylindrical coordinate (r, θ, z) system. Axial (u_z) and radial (u_r) velocity components are non-dimensionalized using a suitably chosen reference velocity, $U_{z,ref}$. The azimuthal (u_θ) velocity component is non-dimensionalized using $U_{\theta,ref} = SU_{z,ref}$, where S is the flow swirl number. All lengths are normalized by the burner outer diameter. The governing equations for the coherent flow component, $\tilde{\boldsymbol{q}}(r, \theta, z, t) = \left[\tilde{\rho}, \tilde{u}_r, \tilde{u}_\theta, \tilde{u}_z, \tilde{p}\right]^T$, can now be written as follows,

$$\begin{aligned}\left(\mathscr{B} + \mathscr{B}^S\{\tilde{\boldsymbol{q}}\}\right)\frac{\partial \tilde{\boldsymbol{q}}}{\partial t} = &-\mathscr{N}\{\tilde{\boldsymbol{q}}\}\tilde{\boldsymbol{q}} - S\mathscr{N}^S\{\tilde{\boldsymbol{q}}\}\tilde{\boldsymbol{q}} - S^2\mathscr{N}^{SS}\{\tilde{\boldsymbol{q}}\}\tilde{\boldsymbol{q}} \\ &+\mathcal{L}_T\tilde{\boldsymbol{q}} + S\mathcal{L}_T^S\tilde{\boldsymbol{q}} + \epsilon^3\hat{\boldsymbol{q}}_{\boldsymbol{a}}(r, z)\cos(\omega_a t)\end{aligned} \tag{2.2}$$

where, the last term on the right is the imposed forcing term from the axisymmetric thermoaocustic oscillation with a frequency ω_a and spatial amplitude distribution $\hat{\boldsymbol{q}}_{\boldsymbol{a}}$, that is assumed to be weak when compared to leading order contributions from hydrodynamic oscillations. As such, its amplitude is $O(\epsilon^3)$ as shown in eq. 2.2 .

In eq. 2.2, the operators $\mathscr{B}$ and $\mathscr{B}^S\{\tilde{\boldsymbol{q}}\}$ are diagonal matrices with elements $\{1, 0, 0, 0, 0\}$ and $\{0, \rho, S\rho, \rho, 0\}$ respectively and $\mathscr{N}\{\tilde{\boldsymbol{q}}\}$, $\mathscr{N}^S\{\tilde{\boldsymbol{q}}\}$ and $\mathscr{N}^{SS}\{\tilde{\boldsymbol{q}}\}$ are nonlinear operators arising from convective terms. $\mathcal{L}_T$ and $\mathcal{L}_T^S$ in eq. 2.2 are the linear operators arising from the pressure gradient term and molecular and turbulent transport terms. An eddy viscosity model along with the Boussinesq assumption is used to close the turbulent transport term as in prior studies (Manoharan *et al.* 2020; Tammisola & Juniper 2016; Oberleithner *et al.* 2015). The various operators in eq. 2.2 are functions of the quantities presented within the associated braces, { }. Also, solutions to eq. 2.2 must be periodic in θ and obey no-slip conditions at the walls and kinematic compatibility conditions on the flow centerline (Batchelor & Gill 1962). The details of the all the operators used in eq. 2.2 are algebraically complex expressions and are presented in the appendix (eqs. A 3, A 6 and A 7).

We derive a solution to eq. 2.2 accurate up to $O(\epsilon^3)$, composed of oscillatory components whose amplitudes grow slowly to their steady-state oscillation values, using the method of multiple scales (Nayfeh 2008). Thus, we introduce a 'fast' time scale $t_1 = t$, a 'slow' time scale $t_2 = \epsilon^2 t$, and an expansion for $\tilde{\boldsymbol{q}}$ in terms of ϵ as follows,

$$\tilde{\boldsymbol{q}}(r, \theta, z, t_1, t_2) = \boldsymbol{q_0}(r, z) + \epsilon\boldsymbol{q_1}(r, \theta, z, t_1, t_2) + \epsilon^2\boldsymbol{q_2}(r, \theta, z, t_1, t_2) + \epsilon^3\boldsymbol{q_3}(r, \theta, z, t_1, t_2) + ... \tag{2.3}$$

where, $\boldsymbol{q_0}$ is the time-averaged flow state at S_c and each term in the expansion is assumed to depend independently on fast and slow time scales. All the operators in eq. 2.2 are also expanded in powers of ϵ (see eqs. A 11, A 16 and A 21 for details). We then substitute these expansions into eq. 2.2 and compare terms that are coefficients of the same power of ϵ on both sides. This yields a sequence of equations for the functions $\boldsymbol{q_1}$, $\boldsymbol{q_2}$, ..., etc. in eq. 2.3.

At $O(\epsilon)$, the unsteady, linearized Navier-Stokes (LNS) equations for q_1 are obtained

as follows,

$$\left(\mathscr{B}_0\frac{\partial}{\partial t_1}+\mathscr{L}\right)\boldsymbol{q_1}=0 \tag{2.4}$$

where, $\mathscr{L}$ is an operator representing the spatial derivative terms in the LNS equations and depends on $\boldsymbol{q_0}$ and S_c. The details of the operators $\mathscr{B}_0$ and $\mathscr{L}$ are presented in the appendix (eqs. A 2 and A 26 respectively). We decompose $\boldsymbol{q_1}$ into Fourier modes in the azimuthal direction and write the solution to eq. 2.4 as follows,

$$\boldsymbol{q_1}(r,\theta,z,t_1,t_2)=A_1(t_2)\hat{\boldsymbol{q}}_{\boldsymbol{1}}(r,z)e^{i(\theta-\omega_1 t_1)}+A_0(t_2)\hat{\boldsymbol{q}}_{\boldsymbol{0}}(r,z)e^{-i\omega_0 t_1}+c.c. \tag{2.5}$$

where, for the present flow, contributions from an axisymmetric mode ($\hat{\boldsymbol{q}}_{\boldsymbol{0}}$) and a helical mode ($\hat{\boldsymbol{q}}_{\boldsymbol{1}}$) have been retained. Thus, ω_0 and ω_1 are their associated natural frequencies, which are given by the solution to the following eigenvalue problem,

$$(-i\omega_m\mathscr{B}_0+\mathscr{L}_m)\,\hat{\boldsymbol{q}}_{\boldsymbol{m}}(r,z)=0 \tag{2.6}$$

where, the operator $\mathscr{L}_m$ is obtained from $\mathscr{L}$ by the transformation $\partial/\partial\theta\rightarrow im$ and $m=0,1$ for the axisymmetric and helical contributions in eq. 2.5, respectively. The spectral analysis of the experimental data shows that the frequency of the axisymmetric hydrodynamic mode does not depend on the air split. This result suggests that the axisymmetric hydrodynamic mode is not self-excited, i.e., $\omega_{0i}<0$ - the subscript 'i' represents the imaginary part. Accordingly, the thermoacoustic frequency, ω_a can now be written in terms of ω_0 and the difference between S and S_c as follows,

$$\omega_a=\omega_0+\epsilon^2\Omega_a \tag{2.7}$$

where, $\Omega_a\sim O(1)$ and quantifies the extent of de-tuning between the natural oscillation frequency ω_0 and the thermoacoustic frequency ω_a. Next, since S_c is the swirl number at which PVC oscillations originate, ω_1 is neutrally stable, i.e. $\omega_{1i}=0$ (Manoharan *et al.* 2020).

The solution for $\boldsymbol{q_2}$ in eq. 2.3 is determined from the equation obtained by comparing $O(\epsilon^2)$ terms on both sides of eq. 2.2 as follows,

$$\begin{aligned}\boldsymbol{q_2}(r,\theta,z,t_1,t_2)=\;&\Delta_s\hat{\boldsymbol{q}}_{\boldsymbol{\Delta}}+|A_1|^2\hat{\boldsymbol{q}}_{\boldsymbol{A_1A_1^*}}\\&+\left(A_1A_0\hat{\boldsymbol{q}}_{\boldsymbol{A_1A_0}}e^{i\theta}e^{-i(\omega_1+\omega_0)t_1}+A_1A_0^*\hat{\boldsymbol{q}}_{\boldsymbol{A_1A_0^*}}e^{i\theta}e^{-i(\omega_1-\omega_0^*)t_1}+c.c.\right)\\&+\left((A_1)^2\hat{\boldsymbol{q}}_{\boldsymbol{A_1A_1}}e^{2i(\theta-\omega_1t_1)}+(A_0)^2\hat{\boldsymbol{q}}_{\boldsymbol{A_0A_0}}e^{-2i\omega_0t_1}+c.c.\right)\\&+\left(B_1\hat{\boldsymbol{q}}_{\boldsymbol{1}}e^{i(\theta-\omega_1t_1)}+B_0\hat{\boldsymbol{q}}_{\boldsymbol{0}}e^{-i\omega_0t_1}+c.c.\right)\end{aligned} \tag{2.8}$$

where, the first term quantifies the change in the time-averaged flow from its state at S_c, the second term is the time-averaged distortion (to leading order) due to finite amplitude helical oscillations. The third set of terms are due to nonlinear coupling between the helical and axisymmetric modes. Note that this results in helical oscillations at frequencies corresponding to the sum and difference of the thermoacoustic and PVC frequencies. The fourth set of terms are the first harmonic of the helical and axisymmetric oscillations. The last set of terms are the complementary functions of the homogeneous form of eq. 2.2 at $O(\epsilon^2)$. These terms are included here for mathematical completeness and will not contribute to the final steady state oscillatory solution up to $O(\epsilon^3)$.

The amplitudes $A_0(t_2)$ and $A_1(t_2)$ are determined from the equation for $\boldsymbol{q_3}$ (coefficient of ϵ^3 in eq. 2.3). This equation has oscillatory source terms of the form $e^{i\omega_0t_1}$ and $e^{-i\omega_1t_1}$, which in general yield terms in the solution for q_3 whose value grows exponentially with

time. Thus, a bounded solution is possible only when the coefficients of these secular terms vanish. This condition yields evolution equations for $A_0(t_2)$ and $A_1(t_2)$ as follows,

$$\frac{dA_0}{dt_2} = \Delta_s \alpha_{A_0} A_0 - \beta_{A_0 A_1} |A_1|^2 A_0 + \beta_{A_0 f} e^{-i\Omega_a t_2} \tag{2.9}$$

$$\frac{dA_1}{dt_2} = \Delta_s \alpha_{A_1} A_1 - \beta_{A_1 A_1} |A_1|^2 A_1 \tag{2.10}$$

where, the coefficients in eqs. 2.9 and 2.10 are determined from inner products between the *adjoint* modes $\hat{\boldsymbol{q}}_{\boldsymbol{0}}^{\dagger}$ and $\hat{\boldsymbol{q}}_{\boldsymbol{1}}^{\dagger}$, and expressions involving various the functions appearing in eqs. 2.5 and 2.8. These expressions are given in the appendix (eqs. B 1 - B 5). Equation 2.10 is equivalent to that derived by Manoharan *et al.* (2020) for the evolution of helical mode oscillations in an unforced flow with constant density. This shows that in the limit of weak axisymmetric forcing, the evolution of A_1, i.e., helical oscillations, is independent of A_0, i.e., the hydrodynamic response to the thermoacoustic forcing. On the other hand, the second term in eq. 2.9 shows that helical oscillations can influence the evolution of the axisymmetric hydrodynamic response. The efficiency with which this occurs is determined by the value of $\beta_{A_0 A_1}$.

The steady-state oscillation amplitudes are determined as follows. First, we introduce $A_0(t_2) = D_0(t_2)\exp[i\phi_0(t_2)]$ and $A_1(t_2) = D_1(t_2)\exp[i\phi_1(t_2)]$ in eqs. 2.9 and 2.10, and equate real and imaginary parts on both sides. The real parts define evolution equations for D_1 and D_0. Requiring time derivatives of D_0 and D_1 to vanish in these equations yields solutions for the steady-state amplitudes. The imaginary parts then yields expressions for the natural frequencies of the axisymmetric and helical modes at S to leading order in $S - S_c$.

The solutions for the steady-state amplitude of the helical mode and its characteristic frequency are as follows,

$$A_{PVC} = \sqrt{\frac{(S - S_c)\alpha_{A_1 r}}{\beta_{A_1 A_1 r}}} \tag{2.11}$$

and,

$$\omega_{PVC} = \omega_1 + (S - S_c)\left(\alpha_{A_1 r}\frac{\beta_{A_1 A_1 i}}{\beta_{A_1 A_1 r}} - \alpha_{A_1 i}\right) \tag{2.12}$$

where, the letters 'r' and 'i' in the subscripts denote real and imaginary parts. Note that as may be expected, the results in eqs. 2.11 and 2.12 are analogous to those derived by Manoharan *et al.* (2020) for a constant density flow.

For the axisymmetric mode, the steady-state oscillation frequency is simply the thermoacoustic frequency ω_a. The steady state amplitude, A_{TH} of the axisymmetric mode is given by the following,

$$A_{TH} = \frac{|\beta_{A_0 f}|}{\left| i\left[\omega_a - \omega_0 - i(S - S_c)\alpha_{A_0}\right] - \beta_{A_0 A_1} A_{PVC}^2 \right|} \tag{2.13}$$

where $\beta_{A_0 f}$ is given as follows:

$$\beta_{A_0 f} = \frac{\langle \hat{\boldsymbol{q}}_{\boldsymbol{0}}^{\dagger}, \hat{\boldsymbol{q}}_{\boldsymbol{a}} \rangle}{2\langle \hat{\boldsymbol{q}}_{\boldsymbol{0}}^{\dagger}, \mathscr{B}_0 \hat{\boldsymbol{q}}_{\boldsymbol{0}} \rangle} \tag{2.14}$$

and $\beta_{A_0A_1}$ is given by the following expression:

$$\beta_{A_0A_1} = \frac{1}{\langle \hat{\boldsymbol{q}}_{\boldsymbol{0}}^{\dagger}, \mathscr{B}_0 \hat{\boldsymbol{q}}_{\boldsymbol{0}} \rangle} \Big\langle \hat{\boldsymbol{q}}^{\boldsymbol{0}\dagger}, \Big[\mathbb{I}_{(-1,1)}\{\boldsymbol{q_0}, \hat{\boldsymbol{q}}_{\boldsymbol{1}}^{*}\}\hat{\boldsymbol{q}}_{\boldsymbol{A_1A_0}} + \mathbb{I}_{(1,-1)}\{\boldsymbol{q_0}, \hat{\boldsymbol{q}}_{\boldsymbol{A_1A_0}}\}\hat{\boldsymbol{q}}_{\boldsymbol{1}}^{*} + \mathbb{I}_{(-1,1)}\{\boldsymbol{q_0}, \hat{\boldsymbol{q}}_{\boldsymbol{A_1^*A_0}}\}\hat{\boldsymbol{q}}_{\boldsymbol{1}} + \mathbb{I}_{(1,-1)}\{\boldsymbol{q_0}, \hat{\boldsymbol{q}}_{\boldsymbol{1}}\}\hat{\boldsymbol{q}}_{\boldsymbol{A_1^*A_0}} + \mathbb{I}_{(0,0)}\{\boldsymbol{q_0}, \hat{\boldsymbol{q}}_{\boldsymbol{A_1A_1^*}}\}\hat{\boldsymbol{q}}_{\boldsymbol{0}} + \mathbb{S}_{(0,0)}\{\boldsymbol{q_0}, \hat{\boldsymbol{q}}_{\boldsymbol{0}}\}\hat{\boldsymbol{q}}_{\boldsymbol{A_1A_1^*}} + \mathbb{Q}_0\{\boldsymbol{q_0}, \hat{\boldsymbol{q}}_{\boldsymbol{1}}^{*}, \hat{\boldsymbol{q}}_{\boldsymbol{1}}\}\hat{\boldsymbol{q}}_{\boldsymbol{0}} + \mathbb{Q}_1\{\boldsymbol{q_0}, \hat{\boldsymbol{q}}_{\boldsymbol{1}}^{*}, \hat{\boldsymbol{q}}_{\boldsymbol{0}}\}\hat{\boldsymbol{q}}_{\boldsymbol{1}} + \mathbb{Q}_{-1}\{\boldsymbol{q_0}, \hat{\boldsymbol{q}}_{\boldsymbol{1}}, \hat{\boldsymbol{q}}_{\boldsymbol{0}}\}\hat{\boldsymbol{q}}_{\boldsymbol{1}}^{*} + \mathbb{T}_0\{\boldsymbol{q_0}, \hat{\boldsymbol{q}}_{\boldsymbol{0}}, \hat{\boldsymbol{q}}_{\boldsymbol{1}}, \hat{\boldsymbol{q}}_{\boldsymbol{1}}^{*}, \hat{\boldsymbol{q}}_{\boldsymbol{A_1A_1^*}}, \hat{\boldsymbol{q}}_{\boldsymbol{A_1A_0}}, \hat{\boldsymbol{q}}_{\boldsymbol{A_1^*A_0}}\}\boldsymbol{q_0} \Big] \Big\rangle \tag{2.15}$$

where, the inner product between two functions $\hat{\boldsymbol{p}}_{\boldsymbol{1}}(r,z)$ and $\hat{\boldsymbol{p}}_{\boldsymbol{2}}(r,z)$ is defined as follows,

$$\langle \hat{\boldsymbol{p}}_{\boldsymbol{1}}, \hat{\boldsymbol{p}}_{\boldsymbol{2}} \rangle = \int_0^Z \int_0^R (\hat{\boldsymbol{p}}_{\boldsymbol{1}})^H \hat{\boldsymbol{p}}_{\boldsymbol{2}}\, r\, dr\, dz \tag{2.16}$$

where, the superscript 'H' denotes the transpose conjugate.

In eq. 2.13, $\beta_{A_0 f}$ quantifies the receptivity of the axisymmetric mode to the forcing imposed by the thermoacosutic oscillations. The denominator in eq. 2.13 quantifies two separate sources of de-tuning. The first term in box brackets in the denominator of eq. 2.13 is the difference between the thermoacoustic forcing and the natural frequency of the axisymmetric mode at S. Thus, as may be expected, a larger difference between these two frequencies results in a smaller response amplitude. The last term in denominator of eq. 2.13 shows that the presence of helical oscillations can additionally reduce A_{TH} if $|\beta_{A_0A_1}|$ is large, i.e., the nonlinear coupling between helical and axisymmetric oscillations is large. From the expression for $\beta_{A_0A_1}$ in eq. 2.15, the contribution from nonlinear coupling between the helical and axisymmetric mode depends on $\hat{\boldsymbol{q}}_{\boldsymbol{A_1^*A_0}}$ and $\hat{\boldsymbol{q}}_{\boldsymbol{A_1A_0}}$. These quantities are components of the solution for $\boldsymbol{q_2}$ (see eq. 2.8) that oscillate with frequencies corresponding to the difference and sum of the helical and axisymmetric oscillations. The equation that determines $\hat{\boldsymbol{q}}_{\boldsymbol{A_1^*A_0}}$ is as follows,

$$\Big(i\Delta\omega\mathscr{B}_0 + \mathscr{L}_{-1}\Big)\hat{\boldsymbol{q}}_{\boldsymbol{A_1^*A_0}} = -\Big(\mathbb{I}_{(0,-1)}\{\boldsymbol{q_0}, \hat{\boldsymbol{q}}_{\boldsymbol{0}}\}\hat{\boldsymbol{q}}_{\boldsymbol{1}}^{*} + \mathbb{I}_{(-1,0)}\{\boldsymbol{q_0}, \hat{\boldsymbol{q}}_{\boldsymbol{1}}^{*}\}\hat{\boldsymbol{q}}_{\boldsymbol{0}} + \mathbb{Q}_0\{\boldsymbol{q_0}, \hat{\boldsymbol{q}}_{\boldsymbol{0}}, \hat{\boldsymbol{q}}_{\boldsymbol{1}}^{*}\}\boldsymbol{q_0}\Big) \tag{2.17}$$

where, $\Delta\omega = \omega_1 - \omega_0$ and the various operators on the right are given in the appendix (eqs. C 6 and C 5). The solution to eq 2.17 can be written in terms of the eigenfunctions of $\mathscr{L}_{-1}$, $\hat{\boldsymbol{q}}_{\boldsymbol{-1,k}}$, and their adjoints as follows,

$$\hat{\boldsymbol{q}}_{\boldsymbol{A_1^*A_0}} = \sum_k \left[\frac{\Big\langle \hat{\boldsymbol{q}}_{\boldsymbol{-1,k}}^{\dagger}, i\Big(\mathbb{I}_{(0,-1)}\{\boldsymbol{q_0}, \hat{\boldsymbol{q}}_{\boldsymbol{0}}\}\hat{\boldsymbol{q}}_{\boldsymbol{1}}^{*} + \mathbb{I}_{(-1,0)}\{\boldsymbol{q_0}, \hat{\boldsymbol{q}}_{\boldsymbol{1}}^{*}\}\hat{\boldsymbol{q}}_{\boldsymbol{0}} + \mathbb{Q}_0\{\boldsymbol{q_0}, \hat{\boldsymbol{q}}_{\boldsymbol{0}}, \hat{\boldsymbol{q}}_{\boldsymbol{1}}^{*}\}\boldsymbol{q_0}\Big)\Big\rangle}{(\Delta\omega + \omega_{-1,k})\langle \hat{\boldsymbol{q}}_{\boldsymbol{-1,k}}^{\dagger}, \mathscr{B}_0 \hat{\boldsymbol{q}}_{\boldsymbol{-1,k}} \rangle} \hat{\boldsymbol{q}}_{\boldsymbol{-1,k}} \right] \tag{2.18}$$

where, the summation is over the entire eigenspace of $\mathscr{L}_{-1}$. Thus, eq. 2.18 shows that when $\Delta\omega$ is small, i.e., when the axisymmetric and helical mode natural frequencies are close, the magnitude of $\hat{\boldsymbol{q}}_{\boldsymbol{A_1^*A_0}}$ is large. Therefore, when the forcing is near-resonant, i.e., $\omega_a \sim \omega_0$, $\beta_{A_0A_1}$ becomes large when $\omega_1 \sim \omega_a$, resulting in an efficient reduction in the amplitude of the axisymmetric hydrodynamic response as eq. 2.13 suggests.

Thus, the asymptotic solution for the stationary flow state, up to ϵ^3, can be written

by combining eqs. 2.5, 2.8 2.11, 2.12 and 2.13 as follows,

$$\begin{aligned}\tilde{\boldsymbol{q}}(r,\theta,z,t) = \boldsymbol{q_0} &+ (S-S_c)\boldsymbol{q_\Delta} + A_{PVC}^2\boldsymbol{q_{A_1A_1^*}} \\ &+\Big(A_{PVC}\hat{\boldsymbol{q}}_{\boldsymbol{1}}e^{i\theta}e^{-i\omega_{PVC}t} + A_{TH}\hat{\boldsymbol{q}}_{\boldsymbol{0}}e^{-i\omega_a t} + c.c.\Big) \\ &+\Big(A_{PVC}^2\hat{\boldsymbol{q}}_{\boldsymbol{A_1A_1}}e^{2i\theta}e^{-2i\omega_{PVC}t} + A_{TH}^2\hat{\boldsymbol{q}}_{\boldsymbol{A_0A_0}}e^{-2i\omega_a t} + c.c.\Big) \\ &+\Big(A_{PVC}A_{TH}\hat{\boldsymbol{q}}_{\boldsymbol{A_1A_0}}e^{i\theta}e^{-i(\omega_{PVC}+\omega_a)t} + c.c.\Big) \\ &+\Big(A_{PVC}A_{TH}\hat{\boldsymbol{q}}_{\boldsymbol{A_1^*A_0}}e^{-i\theta}e^{i(\omega_{PVC}-\omega_a)t} + c.c.\Big) \\ &+O\big((S-S_c)^{3/2}\big)\end{aligned} \tag{2.19}$$

where, t_1 and t_2 have been replaced by t. It is now evident from eq. 2.19 that in general, the flow solution must have oscillating components at the thermoacoustic frequency, the PVC frequency, and their sum and difference. The suppression of the axisymmetric hydrodynamic response to acoustic forcing, due to the presence of a PVC, can potentially result in the suppression of the component of global heat release oscillation due to burning area oscillations in the case of an axisymmetric flame (Acharya *et al.* 2012; Moeck *et al.* 2012). Therefore, ensuring that the characteristic frequency of PVC oscillations in a combustor nozzle matches those of potentially unstable thermoacoustic modes during initial stages of design might prove beneficial because the presence of a suitably designed PVC could suppress global heat release rate oscillations through the nonlinear mechanism described in this section as the qualitative agreement between flow dynamics in the present experimental study and the theory shows.

Appendix A. Governing equations in the operator form

The governing equations for $\tilde{\boldsymbol{q}} = \left[\tilde{\rho}, \tilde{u}_r, \tilde{u}_\theta, \tilde{u}_z, \tilde{p}\right]^T$ i.e. the coherent flow components are represented in the operator form as given in Eq. 2.2. The operators $\mathscr{B}$ and $\mathscr{B}^S\{\tilde{\boldsymbol{q}}\}$ are diagonal matrices with elements $\mathscr{B} = \begin{bmatrix}1 & 0 & 0 & 0 & 0\end{bmatrix}$ and $\mathscr{B}^s\{\tilde{\boldsymbol{q}}\} = \begin{bmatrix}0 & \tilde{\rho} & S\tilde{\rho} & \tilde{\rho} & 0\end{bmatrix}$. The operator $\mathscr{B}^S\{\tilde{\boldsymbol{q}}\}$ can then be expanded as follows:

$$\mathscr{B}^S\{\tilde{\boldsymbol{q}}\} = \mathscr{B}_1^S\{\tilde{\boldsymbol{q}}\} + \epsilon^2\Delta_s\mathscr{B}_2^S\{\tilde{\boldsymbol{q}}\} \tag{A 1}$$

where, $\mathscr{B}_1^S\{\tilde{\boldsymbol{q}}\}$ and $\mathscr{B}_2^S\{\tilde{\boldsymbol{q}}\}$ are diagonal matrices with elements $\mathscr{B}_1^S\{\tilde{\boldsymbol{q}}\} = \begin{bmatrix}0 & \tilde{\rho} & S_c\tilde{\rho} & \tilde{\rho} & 0\end{bmatrix}$ and $\mathscr{B}_2^S\{\tilde{\boldsymbol{q}}\} = \begin{bmatrix}0 & 0 & \tilde{\rho} & 0 & 0\end{bmatrix}$. The matrix $\mathscr{B}_0$ is defined as:

$$\mathscr{B}_0 = \mathscr{B} + \mathscr{B}_1^S\{\boldsymbol{q_0}\} \tag{A 2}$$

The nonlinear operators $\mathscr{N}\{\tilde{\boldsymbol{q}}\}$, $\mathscr{N}^S\{\tilde{\boldsymbol{q}}\}$ and $\mathscr{N}^{SS}\{\tilde{\boldsymbol{q}}\}$ in eq. 2.2 acting on the vector field $\tilde{\boldsymbol{q}}$, are defined as follows:

$$\mathscr{N}\{\tilde{\boldsymbol{q}}\} = \mathscr{N}_1\{\tilde{\boldsymbol{q}}\} + \mathscr{R}_{2,4}^\rho\{\tilde{\boldsymbol{q}}\}\mathscr{N}_2\{\tilde{\boldsymbol{q}}\} + \mathscr{R}_5^\rho\{\tilde{\boldsymbol{q}}\}\mathscr{R}_5^\rho\{\tilde{\boldsymbol{q}}\}\mathscr{N}_3\{\tilde{\boldsymbol{q}}\} \tag{A 3}$$

where,

$$\mathscr{N}_1\{\tilde{\boldsymbol{q}}\} = \begin{bmatrix} \tilde{\Delta}_{rz} & \tilde{\rho}\left(\frac{1}{r}+\frac{\partial}{\partial r}\right) & 0 & \tilde{\rho}\frac{\partial}{\partial z} & 0 \\ 0 & 0 & 0 & 0 & 0 \\ 0 & 0 & 0 & 0 & 0 \\ 0 & 0 & 0 & 0 & 0 \\ \frac{1}{RePr}\left[\tilde{\rho}\Lambda_{r\theta z} - 2\left(\frac{\partial\tilde{\rho}}{\partial r}\frac{\partial}{\partial r}+\frac{1}{r^2}\frac{\partial\tilde{\rho}}{\partial\theta}\frac{\partial}{\partial\theta}+\frac{\partial\tilde{\rho}}{\partial z}\frac{\partial}{\partial z}\right)\right] & 0 & 0 & 0 & 0 \end{bmatrix} \tag{A 4}$$

$$\mathscr{N}_2\{\tilde{\boldsymbol{q}}\} = \begin{bmatrix} 0 & 0 & 0 & 0 & 0 \\ 0 & \tilde{\Delta}_{rz} & 0 & 0 & 0 \\ 0 & 0 & 0 & 0 & 0 \\ 0 & 0 & 0 & \tilde{\Delta}_{rz} & 0 \\ 0 & 0 & 0 & 0 & 0 \end{bmatrix} \quad \mathscr{N}_3\{\tilde{\boldsymbol{q}}\} = \begin{bmatrix} 0 & 0 & 0 & 0 & 0 \\ 0 & 0 & 0 & 0 & 0 \\ 0 & 0 & 0 & 0 & 0 \\ 0 & 0 & 0 & 0 & 0 \\ 0 & \tilde{\rho}\left(\frac{\partial}{\partial r}+\frac{1}{r}\right) & 0 & \tilde{\rho}\frac{\partial}{\partial z} & 0 \end{bmatrix} \tag{A 5}$$

Similarly, we can write $\mathscr{N}^S\{\tilde{\boldsymbol{q}}\}$ and $\mathscr{N}^{SS}\{\tilde{\boldsymbol{q}}\}$ as follows:

$$\mathscr{N}^S\{\tilde{\boldsymbol{q}}\} = \mathscr{N}_1{}^S\{\tilde{\boldsymbol{q}}\} + \mathscr{R}^{\rho}_{2,3,4}\{\tilde{\boldsymbol{q}}\}\mathscr{N}_2{}^S\{\tilde{\boldsymbol{q}}\} + \mathscr{R}^{\rho}_5\{\tilde{\boldsymbol{q}}\}\mathscr{R}^{\rho}_5\{\tilde{\boldsymbol{q}}\}\mathscr{N}_3{}^S\{\tilde{\boldsymbol{q}}\} \tag{A 6}$$

$$\mathscr{N}^{SS}\{\tilde{\boldsymbol{q}}\} = \mathscr{R}^{\rho}_{2,3}\{\tilde{\boldsymbol{q}}\}\mathscr{N}_2{}^{SS}\{\tilde{\boldsymbol{q}}\} \tag{A 7}$$

where,

$$\mathscr{N}_1{}^S\{\tilde{\boldsymbol{q}}\} = \begin{bmatrix} \frac{\tilde{u}_\theta}{r}\frac{\partial}{\partial\theta} & 0 & \frac{\tilde{\rho}}{r}\frac{\partial}{\partial\theta} & 0 & 0 \\ 0 & 0 & 0 & 0 & 0 \\ 0 & 0 & 0 & 0 & 0 \\ 0 & 0 & 0 & 0 & 0 \\ 0 & 0 & 0 & 0 & 0 \end{bmatrix} \quad \mathscr{N}_3{}^S\{\tilde{\boldsymbol{q}}\} = \begin{bmatrix} 0 & 0 & 0 & 0 & 0 \\ 0 & 0 & 0 & 0 & 0 \\ 0 & 0 & 0 & 0 & 0 \\ 0 & 0 & 0 & 0 & 0 \\ 0 & 0 & \frac{\tilde{\rho}}{r}\frac{\partial}{\partial\theta} & 0 & 0 \end{bmatrix} \tag{A 8}$$

$$\mathscr{N}_2{}^S\{\tilde{\boldsymbol{q}}\} = \begin{bmatrix} 0 & 0 & 0 & 0 & 0 \\ 0 & \frac{\tilde{u}_\theta}{r}\frac{\partial}{\partial\theta} & 0 & 0 & 0 \\ 0 & 0 & \left(\tilde{\Delta}_{rz}+\frac{\tilde{u}_r}{r}\right) & 0 & 0 \\ 0 & 0 & 0 & \frac{\tilde{u}_\theta}{r}\frac{\partial}{\partial\theta} & 0 \\ 0 & 0 & 0 & 0 & 0 \end{bmatrix} \tag{A 9}$$

$$\mathscr{N}_2^{SS}\{\tilde{\boldsymbol{q}}\} = \begin{bmatrix} 0 & 0 & 0 & 0 & 0 \\ 0 & 0 & -\frac{\tilde{u}_\theta}{r} & 0 & 0 \\ 0 & 0 & \frac{\tilde{u}_\theta}{r}\frac{\partial}{\partial\theta} & 0 & 0 \\ 0 & 0 & 0 & 0 & 0 \\ 0 & 0 & 0 & 0 & 0 \end{bmatrix} \tag{A 10}$$

where we have defined $\Lambda_{r\theta z} = \left(\frac{\partial^2}{\partial r^2} + \frac{1}{r}\frac{\partial}{\partial r} + \frac{1}{r^2}\frac{\partial^2}{\partial\theta^2} + \frac{\partial^2}{\partial z^2}\right)$ and $\tilde{\Delta}_{rz} = \left(\tilde{u}_r\frac{\partial}{\partial r} + \tilde{u}_z\frac{\partial}{\partial z}\right)$. Also, we define matrix $\mathscr{R}^\rho_{i,j,\ldots}\{\tilde{\boldsymbol{q}}\}$ as a diagonal matrix with non-zero entries as $\tilde{\rho}$ on the $i^{th}, j^{th}, \ldots$ indices. For example, $\mathscr{R}^\rho_{2,4}\{\tilde{\boldsymbol{q}}\}$ is a diagonal matrix with elements: $\begin{bmatrix} 0 & \tilde{\rho} & 0 & \tilde{\rho} & 0 \end{bmatrix}$.

The nonlinear operators can be expanded in powers of ϵ as follows:

$$\mathscr{N}\{\tilde{\boldsymbol{q}}\} = \mathbb{N}^1\{\boldsymbol{q_0}\} + \epsilon\mathbb{N}^\epsilon\{\boldsymbol{q_0}, \boldsymbol{q_1}\} + \epsilon^2\mathbb{N}^{\epsilon^2}\{\boldsymbol{q_0}, \boldsymbol{q_1}, \boldsymbol{q_2}\} + \epsilon^3\mathbb{N}^{\epsilon^3}\{\boldsymbol{q_0}, \boldsymbol{q_1}, \boldsymbol{q_2}, \boldsymbol{q_3}\} + \ldots \tag{A 11}$$

where,

$$\mathbb{N}^1\{\boldsymbol{q_0}\} = \mathscr{N}_1\{\boldsymbol{q_0}\} + \mathscr{R}^\rho_{2,4}\{\boldsymbol{q_0}\}\mathscr{N}_2\{\boldsymbol{q_0}\} + \mathscr{R}^\rho_5\{\boldsymbol{q_0}\}\mathscr{R}^\rho_5\{\boldsymbol{q_0}\}\mathscr{N}_3\{\boldsymbol{q_0}\} \tag{A 12}$$

$$\begin{aligned} \mathbb{N}^\epsilon\{\boldsymbol{q_0}, \boldsymbol{q_1}\} = {} & \mathscr{N}_1\{\boldsymbol{q_1}\} + \mathscr{R}^\rho_{2,4}\{\boldsymbol{q_1}\}\mathscr{N}_2\{\boldsymbol{q_0}\} + \mathscr{R}^\rho_{2,4}\{\boldsymbol{q_0}\}\mathscr{N}_2\{\boldsymbol{q_1}\} \\ & + 2\mathscr{R}^\rho_5\{\boldsymbol{q_0}\}\mathscr{R}^\rho_5\{\boldsymbol{q_1}\}\mathscr{N}_3\{\boldsymbol{q_0}\} + \mathscr{R}^\rho_5\{\boldsymbol{q_0}\}\mathscr{R}^\rho_5\{\boldsymbol{q_0}\}\mathscr{N}_3\{\boldsymbol{q_1}\} \end{aligned} \tag{A 13}$$

$$\begin{aligned} \mathbb{N}^{\epsilon^2}\{\boldsymbol{q_0}, \boldsymbol{q_1}, \boldsymbol{q_2}\} = {} & \mathscr{N}_1\{\boldsymbol{q_2}\} + \mathscr{R}^\rho_{2,4}\{\boldsymbol{q_2}\}\mathscr{N}_2\{\boldsymbol{q_0}\} + \mathscr{R}^\rho_{2,4}\{\boldsymbol{q_0}\}\mathscr{N}_2\{\boldsymbol{q_2}\} \\ & + 2\mathscr{R}^\rho_5\{\boldsymbol{q_0}\}\mathscr{R}^\rho_5\{\boldsymbol{q_2}\}\mathscr{N}_3\{\boldsymbol{q_0}\} + \mathscr{R}^\rho_5\{\boldsymbol{q_0}\}\mathscr{R}^\rho_5\{\boldsymbol{q_0}\}\mathscr{N}_3\{\boldsymbol{q_2}\} \\ & + \mathscr{R}^\rho_{2,4}\{\boldsymbol{q_1}\}\mathscr{N}_2\{\boldsymbol{q_1}\} + 2\mathscr{R}^\rho_5\{\boldsymbol{q_0}\}\mathscr{R}^\rho_5\{\boldsymbol{q_1}\}\mathscr{N}_3\{\boldsymbol{q_1}\} \\ & + \mathscr{R}^\rho_5\{\boldsymbol{q_1}\}\mathscr{R}^\rho_5\{\boldsymbol{q_1}\}\mathscr{N}_3\{\boldsymbol{q_0}\} \end{aligned} \tag{A 14}$$

$$\begin{aligned} \mathbb{N}^{\epsilon^3}\{\boldsymbol{q_0}, \boldsymbol{q_1}, \boldsymbol{q_2}, \boldsymbol{q_3}\} = {} & \mathscr{N}_1\{\boldsymbol{q_3}\} + \mathscr{R}^\rho_{2,4}\{\boldsymbol{q_3}\}\mathscr{N}_2\{\boldsymbol{q_0}\} + \mathscr{R}^\rho_{2,4}\{\boldsymbol{q_0}\}\mathscr{N}_2\{\boldsymbol{q_3}\} \\ & + 2\mathscr{R}^\rho_5\{\boldsymbol{q_0}\}\mathscr{R}^\rho_5\{\boldsymbol{q_3}\}\mathscr{N}_3\{\boldsymbol{q_0}\} + \mathscr{R}^\rho_5\{\boldsymbol{q_0}\}\mathscr{R}^\rho_5\{\boldsymbol{q_0}\}\mathscr{N}_3\{\boldsymbol{q_3}\} \\ & + \mathscr{R}^\rho_{2,4}\{\boldsymbol{q_1}\}\mathscr{N}_2\{\boldsymbol{q_2}\} + 2\mathscr{R}^\rho_5\{\boldsymbol{q_0}\}\mathscr{R}^\rho_5\{\boldsymbol{q_1}\}\mathscr{N}_3\{\boldsymbol{q_2}\} \\ & + \mathscr{R}^\rho_5\{\boldsymbol{q_1}\}\mathscr{R}^\rho_5\{\boldsymbol{q_2}\}\mathscr{N}_3\{\boldsymbol{q_0}\} + \mathscr{R}^\rho_{2,4}\{\boldsymbol{q_2}\}\mathscr{N}_2\{\boldsymbol{q_1}\} \\ & + 2\mathscr{R}^\rho_5\{\boldsymbol{q_0}\}\mathscr{R}^\rho_5\{\boldsymbol{q_2}\}\mathscr{N}_3\{\boldsymbol{q_1}\} + \mathscr{R}^\rho_5\{\boldsymbol{q_2}\}\mathscr{R}^\rho_5\{\boldsymbol{q_1}\}\mathscr{N}_3\{\boldsymbol{q_0}\} \\ & + \mathscr{R}^\rho_5\{\boldsymbol{q_1}\}\mathscr{R}^\rho_5\{\boldsymbol{q_1}\}\mathscr{N}_3\{\boldsymbol{q_1}\} \end{aligned} \tag{A 15}$$

Similarly,

$$\mathscr{N}^S\{\tilde{\boldsymbol{q}}\} = \mathbb{N}^{S,1}\{\boldsymbol{q_0}\} + \epsilon\mathbb{N}^{S,\epsilon}\{\boldsymbol{q_0}, \boldsymbol{q_1}\} + \epsilon^2\mathbb{N}^{S,\epsilon^2}\{\boldsymbol{q_0}, \boldsymbol{q_1}, \boldsymbol{q_2}\} + \epsilon^3\mathbb{N}^{S,\epsilon^3}\{\boldsymbol{q_0}, \boldsymbol{q_1}, \boldsymbol{q_2}, \boldsymbol{q_3}\} + \ldots \tag{A 16}$$

where,

$$\mathbb{N}^{S,1}\{\boldsymbol{q_0}\} = \mathscr{N}_1^S\{\boldsymbol{q_0}\} + \mathscr{R}^\rho_{2,3,4}\{\boldsymbol{q_0}\}\mathscr{N}_2^S\{\boldsymbol{q_0}\} + \mathscr{R}^\rho_5\{\boldsymbol{q_0}\}\mathscr{R}^\rho_5\{\boldsymbol{q_0}\}\mathscr{N}_3^S\{\boldsymbol{q_0}\} \tag{A 17}$$

$$\begin{aligned}\mathbb{N}^{S,\epsilon}\{\boldsymbol{q_0},\boldsymbol{q_1}\} = {}& \mathscr{N}_1^S\{\boldsymbol{q_1}\} + \mathscr{R}^\rho_{2,3,4}\{\boldsymbol{q_1}\}\mathscr{N}_2^S\{\boldsymbol{q_0}\} + \mathscr{R}^\rho_{2,3,4}\{\boldsymbol{q_0}\}\mathscr{N}_2^S\{\boldsymbol{q_1}\} \\ & + 2\mathscr{R}^\rho_5\{\boldsymbol{q_0}\}\mathscr{R}^\rho_5\{\boldsymbol{q_1}\}\mathscr{N}_3^S\{\boldsymbol{q_0}\} + \mathscr{R}^\rho_5\{\boldsymbol{q_0}\}\mathscr{R}^\rho_5\{\boldsymbol{q_0}\}\mathscr{N}_3^S\{\boldsymbol{q_1}\}\end{aligned} \tag{A 18}$$

$$\begin{aligned}\mathbb{N}^{S,\epsilon^2}\{\boldsymbol{q_0},\boldsymbol{q_1},\boldsymbol{q_2}\} = {}& \mathscr{N}_1^S\{\boldsymbol{q_2}\} + \mathscr{R}^\rho_{2,3,4}\{\boldsymbol{q_2}\}\mathscr{N}_2^S\{\boldsymbol{q_0}\} + \mathscr{R}^\rho_{2,3,4}\{\boldsymbol{q_0}\}\mathscr{N}_2^S\{\boldsymbol{q_2}\} \\ & + 2\mathscr{R}^\rho_5\{\boldsymbol{q_0}\}\mathscr{R}^\rho_5\{\boldsymbol{q_2}\}\mathscr{N}_3^S\{\boldsymbol{q_0}\} + \mathscr{R}^\rho_5\{\boldsymbol{q_0}\}\mathscr{R}^\rho_5\{\boldsymbol{q_0}\}\mathscr{N}_3^S\{\boldsymbol{q_2}\} \\ & + \mathscr{R}^\rho_{2,3,4}\{\boldsymbol{q_1}\}\mathscr{N}_2^S\{\boldsymbol{q_1}\} + 2\mathscr{R}^\rho_5\{\boldsymbol{q_0}\}\mathscr{R}^\rho_5\{\boldsymbol{q_1}\}\mathscr{N}_3^S\{\boldsymbol{q_1}\} \\ & + \mathscr{R}^\rho_5\{\boldsymbol{q_1}\}\mathscr{R}^\rho_5\{\boldsymbol{q_1}\}\mathscr{N}_3^S\{\boldsymbol{q_0}\}\end{aligned} \tag{A 19}$$

$$\begin{aligned}\mathbb{N}^{S,\epsilon^3}\{\boldsymbol{q_0},\boldsymbol{q_1},\boldsymbol{q_2},\boldsymbol{q_3}\} = {}& \mathscr{N}_1^S\{\boldsymbol{q_3}\} + \mathscr{R}^\rho_{2,3,4}\{\boldsymbol{q_3}\}\mathscr{N}_2^S\{\boldsymbol{q_0}\} + \mathscr{R}^\rho_{2,3,4}\{\boldsymbol{q_0}\}\mathscr{N}_2^S\{\boldsymbol{q_3}\} \\ & + 2\mathscr{R}^\rho_5\{\boldsymbol{q_0}\}\mathscr{R}^\rho_5\{\boldsymbol{q_3}\}\mathscr{N}_3^S\{\boldsymbol{q_0}\} + \mathscr{R}^\rho_5\{\boldsymbol{q_0}\}\mathscr{R}^\rho_5\{\boldsymbol{q_0}\}\mathscr{N}_3^S\{\boldsymbol{q_3}\} \\ & + \mathscr{R}^\rho_{2,3,4}\{\boldsymbol{q_1}\}\mathscr{N}_2^S\{\boldsymbol{q_2}\} + 2\mathscr{R}^\rho_5\{\boldsymbol{q_0}\}\mathscr{R}^\rho_5\{\boldsymbol{q_1}\}\mathscr{N}_3^S\{\boldsymbol{q_2}\} \\ & + \mathscr{R}^\rho_5\{\boldsymbol{q_1}\}\mathscr{R}^\rho_5\{\boldsymbol{q_2}\}\mathscr{N}_3^S\{\boldsymbol{q_0}\} + \mathscr{R}^\rho_{2,3,4}\{\boldsymbol{q_2}\}\mathscr{N}_2^S\{\boldsymbol{q_1}\} \\ & + 2\mathscr{R}^\rho_5\{\boldsymbol{q_0}\}\mathscr{R}^\rho_5\{\boldsymbol{q_2}\}\mathscr{N}_3^S\{\boldsymbol{q_1}\} + \mathscr{R}^\rho_5\{\boldsymbol{q_2}\}\mathscr{R}^\rho_5\{\boldsymbol{q_1}\}\mathscr{N}_3^S\{\boldsymbol{q_0}\} \\ & + \mathscr{R}^\rho_5\{\boldsymbol{q_1}\}\mathscr{R}^\rho_5\{\boldsymbol{q_1}\}\mathscr{N}_3^S\{\boldsymbol{q_1}\}\end{aligned} \tag{A 20}$$

$\mathscr{N}^{SS}\{\tilde{\boldsymbol{q}}\}$ is also expanded in similar way:

$$\mathscr{N}^{SS}\{\tilde{\boldsymbol{q}}\} = \mathbb{N}^{SS,1}\{\boldsymbol{q_0}\} + \epsilon\mathbb{N}^{SS,\epsilon}\{\boldsymbol{q_0},\boldsymbol{q_1}\} + \epsilon^2\mathbb{N}^{SS,\epsilon^2}\{\boldsymbol{q_0},\boldsymbol{q_1},\boldsymbol{q_2}\} + \epsilon^3\mathbb{N}^{SS,\epsilon^3}\{\boldsymbol{q_0},\boldsymbol{q_1},\boldsymbol{q_2},\boldsymbol{q_3}\} + ... \tag{A 21}$$

where,

$$\mathbb{N}^{SS,1}\{\boldsymbol{q_0}\} = \mathscr{R}^\rho_{2,3}\{\boldsymbol{q_0}\}\mathscr{N}_2^{SS}\{\boldsymbol{q_0}\} \tag{A 22}$$

$$\mathbb{N}^{SS,\epsilon}\{\boldsymbol{q_0},\boldsymbol{q_1}\} = \mathscr{R}^\rho_{2,3}\{\boldsymbol{q_0}\}\mathscr{N}_2^{SS}\{\boldsymbol{q_1}\} + \mathscr{R}^\rho_{2,3}\{\boldsymbol{q_1}\}\mathscr{N}_2^{SS}\{\boldsymbol{q_0}\} \tag{A 23}$$

$$\mathbb{N}^{SS,\epsilon^2}\{\boldsymbol{q_0},\boldsymbol{q_1},\boldsymbol{q_2}\} = \mathscr{R}^\rho_{2,3}\{\boldsymbol{q_0}\}\mathscr{N}_2^{SS}\{\boldsymbol{q_2}\} + \mathscr{R}^\rho_{2,3}\{\boldsymbol{q_2}\}\mathscr{N}_2^{SS}\{\boldsymbol{q_0}\} + \mathscr{R}^\rho_{2,3}\{\boldsymbol{q_1}\}\mathscr{N}_2^{SS}\{\boldsymbol{q_1}\} \tag{A 24}$$

$$\begin{aligned}\mathbb{N}^{SS,\epsilon^3}\{\boldsymbol{q_0},\boldsymbol{q_1},\boldsymbol{q_2},\boldsymbol{q_3}\} = {}& \mathscr{R}^\rho_{2,3}\{\boldsymbol{q_0}\}\mathscr{N}_2^{SS}\{\boldsymbol{q_3}\} + \mathscr{R}^\rho_{2,3}\{\boldsymbol{q_3}\}\mathscr{N}_2^{SS}\{\boldsymbol{q_0}\} \\ & + \mathscr{R}^\rho_{2,3}\{\boldsymbol{q_1}\}\mathscr{N}_2^{SS}\{\boldsymbol{q_2}\} + \mathscr{R}^\rho_{2,3}\{\boldsymbol{q_2}\}\mathscr{N}_2^{SS}\{\boldsymbol{q_1}\}\end{aligned} \tag{A 25}$$

We define the linearized Navier-Stokes operator i.e. $\mathscr{L}$ acting on any vector field $\boldsymbol{p}$ as follows:

$$\begin{aligned}\mathscr{L}\boldsymbol{p} = {}& \big(\mathbb{N}^1\{\boldsymbol{q_0}\}\boldsymbol{p} + \mathbb{N}^\epsilon\{\boldsymbol{q_0},\boldsymbol{p}\}\boldsymbol{q_0}\big) + S_c\big(\mathbb{N}^{S,1}\{\boldsymbol{q_0}\}\boldsymbol{p} + \mathbb{N}^{S,\epsilon}\{\boldsymbol{q_0},\boldsymbol{p}\}\boldsymbol{q_0}\big) \\ & + S_c^2\big(\mathbb{N}^{SS,1}\{\boldsymbol{q_0}\}\boldsymbol{p} + \mathbb{N}^{SS,\epsilon}\{\boldsymbol{q_0},\boldsymbol{p}\}\boldsymbol{q_0}\big) - \big(\mathcal{L}_T\boldsymbol{p} + S_c\mathcal{L}_T^S\boldsymbol{p}\big)\end{aligned} \tag{A 26}$$

We define the vector field $\boldsymbol{p}(r,\theta,z,t_1,t_2) = A_p(t_2)\hat{\boldsymbol{p}}_{\boldsymbol{m}}(r,z)e^{i(m\theta-\omega t_1)}$. The operator $\mathscr{L}_m$ is obtained from $\mathscr{L}$ by the transformation $\partial/\partial\theta \to im$ and the operation $\mathscr{L}_m\hat{\boldsymbol{p}}_{\boldsymbol{m}}$ can be

written as follows:

$$\begin{aligned}\mathscr{L}_m\hat{\boldsymbol{p}}_{\boldsymbol{m}} = \big(\mathbb{N}^1_{(0,m)}\{\boldsymbol{q_0}\}\hat{\boldsymbol{p}}_{\boldsymbol{m}} + \mathbb{N}^{\epsilon}_{(m,0)}\{\boldsymbol{q_0},\hat{\boldsymbol{p}}_{\boldsymbol{m}}\}\boldsymbol{q_0}\big) + S_c\big(\mathbb{N}^{S,1}_{m}\{\boldsymbol{q_0}\}\hat{\boldsymbol{p}}_{\boldsymbol{m}} + \mathbb{N}^{S,\epsilon}_{m}\{\boldsymbol{q_0},\hat{\boldsymbol{p}}_{\boldsymbol{m}}\}\boldsymbol{q_0}\big)\\ + S_c^2\big(\mathbb{N}^{SS,1}_{m}\{\boldsymbol{q_0}\}\hat{\boldsymbol{p}}_{\boldsymbol{m}} + \mathbb{N}^{SS,\epsilon}_{m}\{\boldsymbol{q_0},\hat{\boldsymbol{p}}_{\boldsymbol{m}}\}\boldsymbol{q_0}\big) - \big(\mathcal{L}_{T,m}\hat{\boldsymbol{p}}_{\boldsymbol{m}} + S_c\mathcal{L}^S_{T,m}\hat{\boldsymbol{p}}_{\boldsymbol{m}}\big)\end{aligned} \tag{A 27}$$

We now define following vector fields to explain the various operator-vector operations used in eq. A 27:

$$\begin{aligned}\boldsymbol{r}(r,\theta,z,t_1,t_2) &= A_r(t_2)\hat{\boldsymbol{r}}(r,z)e^{i(r\theta-\omega_r t_1)}\\ \boldsymbol{s}(r,\theta,z,t_1,t_2) &= A_s(t_2)\hat{\boldsymbol{s}}(r,z)e^{i(s\theta-\omega_s t_1)}\end{aligned} \tag{A 28}$$

$\mathbb{N}^1\{\boldsymbol{q_0}\}\boldsymbol{s}$ operation can be expanded as follows:

$$\mathbb{N}^1\{\boldsymbol{q_0}\}\boldsymbol{s} = A_s e^{is\theta}e^{-i\omega_s t_1}\mathbb{N}^1_{(0,s)}\{\boldsymbol{q_0}\}\hat{\boldsymbol{s}} \tag{A 29}$$

Using eq. A 12,

$$\mathbb{N}^1_{(0,s)}\{\boldsymbol{q_0}\}\hat{\boldsymbol{s}} = \mathscr{N}_1^{(0,s)}\{\boldsymbol{q_0}\}\hat{\boldsymbol{s}} + \mathscr{R}^{\rho}_{2,4}\{\boldsymbol{q_0}\}\mathscr{N}_2\{\boldsymbol{q_0}\}\hat{\boldsymbol{s}} + \mathscr{R}^{\rho}_{5}\{\boldsymbol{q_0}\}\mathscr{R}^{\rho}_{5}\{\boldsymbol{q_0}\}\mathscr{N}_3\{\boldsymbol{q_0}\}\hat{\boldsymbol{s}} \tag{A 30}$$

Similarly,

$$\mathbb{N}^{\epsilon}\{\boldsymbol{q_0},\boldsymbol{r}\}\boldsymbol{s} = A_r A_s e^{i(r+s)\theta}e^{-i(\omega_r+\omega_s)t_1}\mathbb{N}^{\epsilon}_{(r,s)}\{\boldsymbol{q_0},\hat{\boldsymbol{r}}\}\hat{\boldsymbol{s}} \tag{A 31}$$

Using eq. A 13,

$$\begin{aligned}\mathbb{N}^{\epsilon}_{(r,s)}\{\boldsymbol{q_0},\boldsymbol{r}\}\boldsymbol{s} = \mathscr{N}_1^{(r,s)}\{\hat{\boldsymbol{r}}\}\hat{\boldsymbol{s}} + \mathscr{R}^{\rho}_{2,4}\{\boldsymbol{q_0}\}\mathscr{N}_2\{\hat{\boldsymbol{r}}\}\hat{\boldsymbol{s}} + \mathscr{R}^{\rho}_{2,4}\{\hat{\boldsymbol{r}}\}\mathscr{N}_2\{\boldsymbol{q_0}\}\hat{\boldsymbol{s}}\\ + 2\mathscr{R}^{\rho}_{5}\{\boldsymbol{q_0}\}\mathscr{R}^{\rho}_{5}\{\hat{\boldsymbol{r}}\}\mathscr{N}_3\{\boldsymbol{q_0}\}\hat{\boldsymbol{s}} + \mathscr{R}^{\rho}_{5}\{\boldsymbol{q_0}\}\mathscr{R}^{\rho}_{5}\{\boldsymbol{q_0}\}\mathscr{N}_3\{\hat{\boldsymbol{r}}\}\hat{\boldsymbol{s}}\end{aligned} \tag{A 32}$$

The matrix-vector operation $\mathscr{N}_1^{(r,s)}\{\hat{\boldsymbol{r}}\}\hat{\boldsymbol{s}}$ is obtained by setting $\partial\tilde{\rho}/\partial\theta = ir\tilde{\rho}$ in the first element of last row and $\partial/\partial\theta = is$ in the expression for $\mathscr{N}_1\{\tilde{\boldsymbol{q}}\}$ in eq. A 3.

Similarly, we expand the various other operations used in eq. A 27 using eqs. A 17, A 18, A 22 and A 23 as follows:

$$\mathbb{N}^{S,1}_{s}\{\boldsymbol{q_0}\}\hat{\boldsymbol{s}} = \mathscr{N}_1^{S,s}\{\boldsymbol{q_0}\}\hat{\boldsymbol{s}} + \mathscr{R}^{\rho}_{5}\{\hat{\boldsymbol{p}}\}\mathscr{N}_2^{S,s}\{\boldsymbol{q_0}\}\hat{\boldsymbol{s}} + \mathscr{R}^{\rho}_{5}\{\boldsymbol{q_0}\}\mathscr{R}^{\rho}_{5}\{\boldsymbol{q_0}\}\mathscr{N}_3^{S,s}\{\boldsymbol{q_0}\}\hat{\boldsymbol{s}} \tag{A 33}$$

$$\begin{aligned}\mathbb{N}^{S,\epsilon}_{s}\{\boldsymbol{q_0},\hat{\boldsymbol{r}}\}\hat{\boldsymbol{s}} = \mathscr{N}_1^{S,s}\{\hat{\boldsymbol{r}}\}\hat{\boldsymbol{s}} + \mathscr{R}^{\rho}_{2,3,4}\{\hat{\boldsymbol{r}}\}\mathscr{N}_2^{S,s}\{\boldsymbol{q_0}\}\hat{\boldsymbol{s}} + \mathscr{R}^{\rho}_{2,3,4}\{\boldsymbol{q_0}\}\mathscr{N}_2^{S,s}\{\hat{\boldsymbol{r}}\}\hat{\boldsymbol{s}}\\ +2\mathscr{R}^{\rho}_{5}\{\boldsymbol{q_0}\}\mathscr{R}^{\rho}_{5}\{\hat{\boldsymbol{r}}\}\mathscr{N}_3^{S,s}\{\boldsymbol{q_0}\}\hat{\boldsymbol{s}} + \mathscr{R}^{\rho}_{5}\{\boldsymbol{q_0}\}\mathscr{R}^{\rho}_{5}\{\boldsymbol{q_0}\}\mathscr{N}_3^{S,s}\{\hat{\boldsymbol{r}}\}\hat{\boldsymbol{s}}\end{aligned} \tag{A 34}$$

$$\mathbb{N}^{SS,1}_{s}\{\boldsymbol{q_0}\}\hat{\boldsymbol{s}} = \mathscr{R}^{\rho}_{2,3}\{\boldsymbol{q_0}\}\mathscr{N}_2^{SS,s}\{\boldsymbol{q_0}\}\hat{\boldsymbol{s}} \tag{A 35}$$

$$\mathbb{N}^{SS,\epsilon}_{s}\{\boldsymbol{q_0},\hat{\boldsymbol{r}}\}\hat{\boldsymbol{s}} = \mathscr{R}^{\rho}_{2,3}\{\boldsymbol{q_0}\}\mathscr{N}_2^{SS,s}\{\hat{\boldsymbol{r}}\}\hat{\boldsymbol{s}} + \mathscr{R}^{\rho}_{2,3}\{\hat{\boldsymbol{r}}\}\mathscr{N}_2^{SS,s}\{\boldsymbol{q_0}\}\hat{\boldsymbol{s}} \tag{A 36}$$

Appendix B. Coefficients in the evolution equations of A_1 and A_0

The coefficients in the evolution equation for $A_1(t_2)$ i.e. eq. 2.10 are defined as follows:

$$\begin{aligned}\alpha_{A_1} = \frac{1}{\langle\hat{\boldsymbol{q}}_{\boldsymbol{1}}^{\dagger},\mathscr{B}_0\hat{\boldsymbol{q}}_{\boldsymbol{1}}\rangle}\Big\langle\hat{\boldsymbol{q}}_{\boldsymbol{1}}^{\dagger},-\Big[(-i\omega_1)\mathscr{B}_1^S\{\hat{\boldsymbol{q}}_{\boldsymbol{\Delta}}\}\hat{\boldsymbol{q}}_{\boldsymbol{1}} + \mathbb{S}_{(0,1)}\{\boldsymbol{q_0},\hat{\boldsymbol{q}}_{\boldsymbol{\Delta}}\}\hat{\boldsymbol{q}}_{\boldsymbol{1}} + \mathbb{S}_{(1,0)}\{\boldsymbol{q_0},\hat{\boldsymbol{q}}_{\boldsymbol{1}}\}\hat{\boldsymbol{q}}_{\boldsymbol{\Delta}}\\ + \mathbb{R}_0\{\boldsymbol{q_0},\hat{\boldsymbol{q}}_{\boldsymbol{1}},\hat{\boldsymbol{q}}_{\boldsymbol{\Delta}}\}\boldsymbol{q_0} + \mathbb{R}_0\{\boldsymbol{q_0},\hat{\boldsymbol{q}}_{\boldsymbol{\Delta}},\hat{\boldsymbol{q}}_{\boldsymbol{1}}\}\boldsymbol{q_0} + \mathbb{N}_1^{S,1}\{\boldsymbol{q_0}\}\hat{\boldsymbol{q}}_{\boldsymbol{1}}\\ + 2S_c\mathbb{N}_1^{SS,1}\{\boldsymbol{q_0}\}\hat{\boldsymbol{q}}_{\boldsymbol{1}} - \mathcal{L}^S_{T,0}\hat{\boldsymbol{q}}_{\boldsymbol{1}} + (-i\omega_1)\mathscr{B}_2^S\{\boldsymbol{q_0}\}\hat{\boldsymbol{q}}_{\boldsymbol{1}}\\ + \mathbb{N}_0^{S,\epsilon}\{\boldsymbol{q_0},\hat{\boldsymbol{q}}_{\boldsymbol{1}}\}\boldsymbol{q_0} + 2S_c\mathbb{N}_0^{SS,\epsilon}\{\boldsymbol{q_0},\hat{\boldsymbol{q}}_{\boldsymbol{1}}\}\boldsymbol{q_0}\Big]\Big\rangle\end{aligned} \tag{B 1}$$

$$\begin{aligned}\beta_{A_1A_1} = \frac{1}{\langle \hat{\boldsymbol{q}}_{\boldsymbol{1}}^{\dagger}, \mathscr{B}_0\hat{\boldsymbol{q}}_{\boldsymbol{1}}\rangle}\Big\langle \hat{\boldsymbol{q}}_{\boldsymbol{1}}^{\dagger}, \Big[&\mathbb{I}_{(-1,2)}\{\boldsymbol{q_0}, \hat{\boldsymbol{q}}_{\boldsymbol{1}}^{*}\}\hat{\boldsymbol{q}}_{\boldsymbol{A_1A_1}} + \mathbb{I}_{(0,1)}\{\boldsymbol{q_0}, \hat{\boldsymbol{q}}_{\boldsymbol{A_1A_1^*}}\}\hat{\boldsymbol{q}}_{\boldsymbol{1}} + \mathbb{I}_{(2,-1)}\{\boldsymbol{q_0}, \hat{\boldsymbol{q}}_{\boldsymbol{A_1A_1}}\}\hat{\boldsymbol{q}}_{\boldsymbol{1}} \\ &+ \mathbb{S}_{(1,0)}\{\boldsymbol{q_0}, \hat{\boldsymbol{q}}_{\boldsymbol{1}}\}\hat{\boldsymbol{q}}_{\boldsymbol{A_1A_1^*}} + \mathbb{R}_{-1}\{\boldsymbol{q_0}, \hat{\boldsymbol{q}}_{\boldsymbol{1}}, \hat{\boldsymbol{q}}_{\boldsymbol{1}}\}\hat{\boldsymbol{q}}_{\boldsymbol{1}}^{*} + \mathbb{Q}_1\{\boldsymbol{q_0}, \hat{\boldsymbol{q}}_{\boldsymbol{1}}^{*}, \hat{\boldsymbol{q}}_{\boldsymbol{1}}\}\hat{\boldsymbol{q}}_{\boldsymbol{1}} \\ &+ \mathbb{Q}_0\{\boldsymbol{q_0}, \hat{\boldsymbol{q}}_{\boldsymbol{1}}, \hat{\boldsymbol{q}}_{\boldsymbol{A_1A_1^*}}\}\boldsymbol{q_0} + \mathbb{Q}_0\{\boldsymbol{q_0}, \hat{\boldsymbol{q}}_{\boldsymbol{1}}^{*}, \hat{\boldsymbol{q}}_{\boldsymbol{A_1A_1}}\}\boldsymbol{q_0} + \mathbb{P}^{\epsilon^3}\{\hat{\boldsymbol{q}}_{\boldsymbol{1}}, \hat{\boldsymbol{q}}_{\boldsymbol{1}}, \hat{\boldsymbol{q}}_{\boldsymbol{1}}^{*}\}\boldsymbol{q_0} \\ &+ \mathbb{P}^{\epsilon^3}\{\hat{\boldsymbol{q}}_{\boldsymbol{1}}, \hat{\boldsymbol{q}}_{\boldsymbol{1}}^{*}, \hat{\boldsymbol{q}}_{\boldsymbol{1}}\}\boldsymbol{q_0} + \mathbb{P}^{\epsilon^3}\{\hat{\boldsymbol{q}}_{\boldsymbol{1}}^{*}, \hat{\boldsymbol{q}}_{\boldsymbol{1}}, \hat{\boldsymbol{q}}_{\boldsymbol{1}}\}\boldsymbol{q_0} + S_c\mathbb{P}_0^{S,\epsilon^3}\{\hat{\boldsymbol{q}}_{\boldsymbol{1}}, \hat{\boldsymbol{q}}_{\boldsymbol{1}}, \hat{\boldsymbol{q}}_{\boldsymbol{1}}^{*}\}\boldsymbol{q_0} \\ &+ S_c\mathbb{P}_0^{S,\epsilon^3}\{\hat{\boldsymbol{q}}_{\boldsymbol{1}}, \hat{\boldsymbol{q}}_{\boldsymbol{1}}^{*}, \hat{\boldsymbol{q}}_{\boldsymbol{1}}\}\boldsymbol{q_0} + S_c\mathbb{P}_0^{S,\epsilon^3}\{\hat{\boldsymbol{q}}_{\boldsymbol{1}}^{*}, \hat{\boldsymbol{q}}_{\boldsymbol{1}}, \hat{\boldsymbol{q}}_{\boldsymbol{1}}\}\boldsymbol{q_0}\Big]\Big\rangle\end{aligned} \tag{B 2}$$

The coefficients in the evolution equation for $A_0(t_2)$ i.e. eq. 2.9 are defined as follows:

$$\begin{aligned}\alpha_{A_0} = \frac{1}{\langle \hat{\boldsymbol{q}}_{\boldsymbol{0}}^{\dagger}, \mathscr{B}_0\hat{\boldsymbol{q}}_{\boldsymbol{0}}\rangle}\Big\langle \hat{\boldsymbol{q}}_{\boldsymbol{0}}^{\dagger}, -\Big[&(-i\omega_0)\mathscr{B}_1^S\{\hat{\boldsymbol{q}}_{\boldsymbol{\Delta}}\}\hat{\boldsymbol{q}}_{\boldsymbol{0}} + \mathbb{S}_{(0,0)}\{\boldsymbol{q_0}, \hat{\boldsymbol{q}}_{\boldsymbol{\Delta}}\}\hat{\boldsymbol{q}}_{\boldsymbol{0}} + \mathbb{S}_{(0,0)}\{\boldsymbol{q_0}, \hat{\boldsymbol{q}}_{\boldsymbol{0}}\}\hat{\boldsymbol{q}}_{\boldsymbol{\Delta}} \\ &+ \mathbb{R}_0\{\boldsymbol{q_0}, \hat{\boldsymbol{q}}_{\boldsymbol{0}}, \hat{\boldsymbol{q}}_{\boldsymbol{\Delta}}\}\boldsymbol{q_0} + \mathbb{R}_0\{\boldsymbol{q_0}, \hat{\boldsymbol{q}}_{\boldsymbol{\Delta}}, \hat{\boldsymbol{q}}_{\boldsymbol{0}},\}\boldsymbol{q_0} + \mathbb{N}_1^{S,1}\{\boldsymbol{q_0}\}\hat{\boldsymbol{q}}_{\boldsymbol{0}} \\ &+ 2S_c\mathbb{N}_1^{SS,1}\{\boldsymbol{q_0}\}\hat{\boldsymbol{q}}_{\boldsymbol{0}} - \mathcal{L}_{T,0}^{S}\hat{\boldsymbol{q}}^{\boldsymbol{0}} + (-i\omega_0)\mathscr{B}_2^S\{\boldsymbol{q_0}\}\hat{\boldsymbol{q}}_{\boldsymbol{0}} \\ &+ \mathbb{N}_0^{S,\epsilon}\{\boldsymbol{q_0}, \hat{\boldsymbol{q}}_{\boldsymbol{0}}\}\boldsymbol{q_0} + 2S_c\mathbb{N}_0^{SS,\epsilon}\{\boldsymbol{q_0}, \hat{\boldsymbol{q}}_{\boldsymbol{0}}\}\boldsymbol{q_0}\Big]\Big\rangle\end{aligned} \tag{B 3}$$

$$\beta_{A_0f} = \frac{\langle \hat{\boldsymbol{q}}_{\boldsymbol{0}}^{\dagger}, \hat{\boldsymbol{q}}_{\boldsymbol{a}}\rangle}{2\langle \hat{\boldsymbol{q}}_{\boldsymbol{0}}^{\dagger}, \mathscr{B}_0\hat{\boldsymbol{q}}_{\boldsymbol{0}}\rangle} \tag{B 4}$$

$$\begin{aligned}\beta_{A_0A_1} = \frac{1}{\langle \hat{\boldsymbol{q}}_{\boldsymbol{0}}^{\dagger}, \mathscr{B}_0\hat{\boldsymbol{q}}_{\boldsymbol{0}}\rangle}\Big\langle \hat{\boldsymbol{q}}^{\boldsymbol{0}\dagger}, \Big[&\mathbb{I}_{(-1,1)}\{\boldsymbol{q_0}, \hat{\boldsymbol{q}}_{\boldsymbol{1}}^{*}\}\hat{\boldsymbol{q}}_{\boldsymbol{A_1A_0}} + \mathbb{I}_{(1,-1)}\{\boldsymbol{q_0}, \hat{\boldsymbol{q}}_{\boldsymbol{A_1A_0}}\}\hat{\boldsymbol{q}}_{\boldsymbol{1}}^{*} + \mathbb{I}_{(-1,1)}\{\boldsymbol{q_0}, \hat{\boldsymbol{q}}_{\boldsymbol{A_1^*A_0}}\}\hat{\boldsymbol{q}}_{\boldsymbol{1}} \\ &+ \mathbb{I}_{(1,-1)}\{\boldsymbol{q_0}, \hat{\boldsymbol{q}}_{\boldsymbol{1}}\}\hat{\boldsymbol{q}}_{\boldsymbol{A_1^*A_0}} + \mathbb{I}_{(0,0)}\{\boldsymbol{q_0}, \hat{\boldsymbol{q}}_{\boldsymbol{A_1A_1^*}}\}\hat{\boldsymbol{q}}_{\boldsymbol{0}} + \mathbb{S}_{(0,0)}\{\boldsymbol{q_0}, \hat{\boldsymbol{q}}_{\boldsymbol{0}}\}\hat{\boldsymbol{q}}_{\boldsymbol{A_1A_1^*}} \\ &+ \mathbb{Q}_0\{\boldsymbol{q_0}, \hat{\boldsymbol{q}}_{\boldsymbol{1}}^{*}, \hat{\boldsymbol{q}}_{\boldsymbol{1}}\}\hat{\boldsymbol{q}}_{\boldsymbol{0}} + \mathbb{Q}_1\{\boldsymbol{q_0}, \hat{\boldsymbol{q}}_{\boldsymbol{1}}^{*}, \hat{\boldsymbol{q}}_{\boldsymbol{0}}\}\hat{\boldsymbol{q}}_{\boldsymbol{1}} + \mathbb{Q}_{-1}\{\boldsymbol{q_0}, \hat{\boldsymbol{q}}_{\boldsymbol{1}}, \hat{\boldsymbol{q}}_{\boldsymbol{0}}\}\hat{\boldsymbol{q}}_{\boldsymbol{1}}^{*} \\ &+ \mathbb{T}_0\{\boldsymbol{q_0}, \hat{\boldsymbol{q}}_{\boldsymbol{0}}, \hat{\boldsymbol{q}}_{\boldsymbol{1}}, \hat{\boldsymbol{q}}_{\boldsymbol{1}}^{*}, \hat{\boldsymbol{q}}_{\boldsymbol{A_1A_1^*}}, \hat{\boldsymbol{q}}_{\boldsymbol{A_1A_0}}, \hat{\boldsymbol{q}}_{\boldsymbol{A_1^*A_0}}\}\boldsymbol{q_0}\Big]\Big\rangle\end{aligned} \tag{B 5}$$

Appendix C. Operator definitions

We define following vector fields for describing the various matrix operators used in this paper:

$$\begin{aligned}\tilde{\boldsymbol{p}}(r,\theta,z,t_1,t_2) &= A_p(t_2)\hat{\boldsymbol{p}}(r,z)e^{i(p\theta-\omega_p t_1)} \\ \tilde{\boldsymbol{r}}(r,\theta,z,t_1,t_2) &= A_r(t_2)\hat{\boldsymbol{r}}(r,z)e^{i(r\theta-\omega_r t_1)} \\ \tilde{\boldsymbol{s}}(r,\theta,z,t_1,t_2) &= A_s(t_2)\hat{\boldsymbol{s}}(r,z)e^{i(s\theta-\omega_s t_1)}\end{aligned} \tag{C 1}$$

$$\begin{aligned}\mathbb{T}_0\{\boldsymbol{q_0},\hat{\boldsymbol{q}}_{\boldsymbol{0}},\hat{\boldsymbol{q}}_{\boldsymbol{1}},\hat{\boldsymbol{q}}^{*}_{\boldsymbol{1}},\hat{\boldsymbol{q}}_{\boldsymbol{A_1A_1^*}},\hat{\boldsymbol{q}}_{\boldsymbol{A_1A_0}},\hat{\boldsymbol{q}}_{\boldsymbol{A_1^*A_0}}\}\boldsymbol{q_0} = \Big[&\mathbb{Q}_0\{\boldsymbol{q_0},\hat{\boldsymbol{q}}_{\boldsymbol{0}},\hat{\boldsymbol{q}}_{\boldsymbol{A_1A_1^*}}\}\\ &+\mathbb{Q}_0\{\boldsymbol{q_0},\hat{\boldsymbol{q}}_{\boldsymbol{1}},\hat{\boldsymbol{q}}_{\boldsymbol{A_1^*A_0}}\}+\mathbb{Q}_0\{\boldsymbol{q_0},\hat{\boldsymbol{q}}^{*}_{\boldsymbol{1}},\hat{\boldsymbol{q}}_{\boldsymbol{A_1A_0}}\}\\ &+\mathbb{P}^{\epsilon^3}\{\hat{\boldsymbol{q}}^{\boldsymbol{0}},\hat{\boldsymbol{q}}_{\boldsymbol{1}},\hat{\boldsymbol{q}}^{*}_{\boldsymbol{1}}\}+\mathbb{P}^{\epsilon^3}\{\hat{\boldsymbol{q}}_{\boldsymbol{0}},\hat{\boldsymbol{q}}^{*}_{\boldsymbol{1}},\hat{\boldsymbol{q}}_{\boldsymbol{1}}\}\\ &+\mathbb{P}^{\epsilon^3}\{\hat{\boldsymbol{q}}_{\boldsymbol{1}},\hat{\boldsymbol{q}}_{\boldsymbol{0}},\hat{\boldsymbol{q}}^{*}_{\boldsymbol{1}}\}+\mathbb{P}^{\epsilon^3}\{\hat{\boldsymbol{q}}^{*}_{\boldsymbol{1}},\hat{\boldsymbol{q}}_{\boldsymbol{0}},\hat{\boldsymbol{q}}_{\boldsymbol{1}}\}\\ &+\mathbb{P}^{\epsilon^3}\{\hat{\boldsymbol{q}}_{\boldsymbol{1}},\hat{\boldsymbol{q}}^{*}_{\boldsymbol{1}},\hat{\boldsymbol{q}}_{\boldsymbol{0}}\}+\mathbb{P}^{\epsilon^3}\{\hat{\boldsymbol{q}}^{*}_{\boldsymbol{1}},\hat{\boldsymbol{q}}_{\boldsymbol{1}},\hat{\boldsymbol{q}}_{\boldsymbol{0}}\}\\ &+S_c\big(\mathbb{P}_0^{S,\epsilon^3}\{\hat{\boldsymbol{q}}_{\boldsymbol{0}},\hat{\boldsymbol{q}}_{\boldsymbol{1}},\hat{\boldsymbol{q}}^{*}_{\boldsymbol{1}}\}+\mathbb{P}_0^{S,\epsilon^3}\{\hat{\boldsymbol{q}}_{\boldsymbol{0}},\hat{\boldsymbol{q}}^{*}_{\boldsymbol{1}},\hat{\boldsymbol{q}}_{\boldsymbol{1}}\}\big)\\ &+S_c\big(\mathbb{P}_0^{S,\epsilon^3}\{\hat{\boldsymbol{q}}_{\boldsymbol{1}},\hat{\boldsymbol{q}}_{\boldsymbol{0}},\hat{\boldsymbol{q}}^{*}_{\boldsymbol{1}}\}+\mathbb{P}_0^{S,\epsilon^3}\{\hat{\boldsymbol{q}}^{*}_{\boldsymbol{1}},\hat{\boldsymbol{q}}_{\boldsymbol{0}},\hat{\boldsymbol{q}}_{\boldsymbol{1}}\}\big)\\ &+S_c\big(\mathbb{P}_0^{S,\epsilon^3}\{\hat{\boldsymbol{q}}_{\boldsymbol{1}},\hat{\boldsymbol{q}}^{*}_{\boldsymbol{1}},\hat{\boldsymbol{q}}^{\boldsymbol{0}}\}+\mathbb{P}_0^{S,\epsilon^3}\{\hat{\boldsymbol{q}}^{*}_{\boldsymbol{1}},\hat{\boldsymbol{q}}_{\boldsymbol{1}},\hat{\boldsymbol{q}}_{\boldsymbol{0}}\}\big)\Big]\boldsymbol{q_0}\end{aligned} \tag{C 2}$$

where,

$$\mathbb{P}^{\epsilon^3}\{\hat{\boldsymbol{p}},\hat{\boldsymbol{r}},\hat{\boldsymbol{s}}\}\boldsymbol{q_0} = \mathscr{R}_5^{\rho}\{\hat{\boldsymbol{p}}\}\mathscr{R}_5^{\rho}\{\hat{\boldsymbol{r}}\}\mathscr{N}_3\{\hat{\boldsymbol{s}}\}\boldsymbol{q_0} \tag{C 3}$$

$$\mathbb{P}_0^{S,\epsilon^3}\{\hat{\boldsymbol{p}},\hat{\boldsymbol{r}},\hat{\boldsymbol{s}}\}\boldsymbol{q_0} = \mathscr{R}_5^{\rho}\{\hat{\boldsymbol{p}}\}\mathscr{R}_5^{\rho}\{\hat{\boldsymbol{r}}\}\mathscr{N}_3^{S,0}\{\hat{\boldsymbol{s}}\}\boldsymbol{q_0} \tag{C 4}$$

$$\mathbb{Q}_s\{\boldsymbol{q_0},\hat{\boldsymbol{p}},\hat{\boldsymbol{r}}\}\hat{\boldsymbol{s}} = \mathbb{R}_s\{\boldsymbol{q_0},\hat{\boldsymbol{p}},\hat{\boldsymbol{r}}\}\hat{\boldsymbol{s}} + \mathbb{R}_s\{\boldsymbol{q_0},\hat{\boldsymbol{r}},\hat{\boldsymbol{p}}\}\hat{\boldsymbol{s}} \tag{C 5}$$

$$\mathbb{I}_{(p,r)}\{\boldsymbol{q_0},\hat{\boldsymbol{p}}\}\hat{\boldsymbol{r}} = (-i\omega_r)\mathscr{B}_1^{S}\{\hat{\boldsymbol{p}}\}\hat{\boldsymbol{r}} + \mathbb{S}_{(p,r)}\{\boldsymbol{q_0},\hat{\boldsymbol{p}}\}\hat{\boldsymbol{r}} \tag{C 6}$$

$$\mathbb{R}_s\{\boldsymbol{q_0},\hat{\boldsymbol{p}},\hat{\boldsymbol{r}}\}\hat{\boldsymbol{s}} = \mathbb{P}^{\epsilon^2}\{\boldsymbol{q_0},\hat{\boldsymbol{p}},\hat{\boldsymbol{r}}\}\hat{\boldsymbol{s}} + S_c\mathbb{P}_s^{S,\epsilon^2}\{\boldsymbol{q_0},\hat{\boldsymbol{p}},\hat{\boldsymbol{r}}\}\hat{\boldsymbol{s}} + S_c^2\mathbb{P}_s^{SS,\epsilon^2}\{\hat{\boldsymbol{p}},\hat{\boldsymbol{r}}\}\hat{\boldsymbol{s}} \tag{C 7}$$

$$\mathbb{S}_{(p,r)}\{\boldsymbol{q_0},\hat{\boldsymbol{p}}\}\hat{\boldsymbol{r}} = \mathbb{N}_{(p,r)}^{\epsilon}\{\boldsymbol{q_0},\hat{\boldsymbol{p}}\}\hat{\boldsymbol{r}} + S_c\mathbb{N}_r^{S,\epsilon}\{\boldsymbol{q_0},\hat{\boldsymbol{r}}\}\hat{\boldsymbol{r}} + S_c^2\mathbb{N}_r^{SS,\epsilon}\{\boldsymbol{q_0},\hat{\boldsymbol{p}}\}\hat{\boldsymbol{r}} \tag{C 8}$$

$$\begin{aligned}\mathbb{P}^{\epsilon^2}\{\boldsymbol{q_0},\hat{\boldsymbol{p}},\hat{\boldsymbol{r}}\}\hat{\boldsymbol{s}} = \mathscr{R}_{2,4}^{\rho}\{\hat{\boldsymbol{p}}\}\mathscr{N}_2\{\hat{\boldsymbol{r}}\}\hat{\boldsymbol{s}} + 2\mathscr{R}_5^{\rho}\{\boldsymbol{q_0}\}\mathscr{R}_5^{\rho}\{\hat{\boldsymbol{p}}\}\mathscr{N}_3\{\hat{\boldsymbol{r}}\}\hat{\boldsymbol{s}}\\ + \mathscr{R}_5^{\rho}\{\hat{\boldsymbol{p}}\}\mathscr{R}_5^{\rho}\{\hat{\boldsymbol{r}}\}\mathscr{N}_3\{\boldsymbol{q_0}\}\hat{\boldsymbol{s}}\end{aligned} \tag{C 9}$$

$$\begin{aligned}\mathbb{P}_s^{S,\epsilon^2}\{\boldsymbol{q_0},\hat{\boldsymbol{p}},\hat{\boldsymbol{r}}\}\hat{\boldsymbol{s}} = \mathscr{R}_{2,4}^{\rho}\{\hat{\boldsymbol{p}}\}\mathscr{N}_2^{S,s}\{\hat{\boldsymbol{r}}\}\hat{\boldsymbol{s}} + 2\mathscr{R}_5^{\rho}\{\boldsymbol{q_0}\}\mathscr{R}_5^{\rho}\{\hat{\boldsymbol{p}}\}\mathscr{N}_3^{S,s}\{\hat{\boldsymbol{r}}\}\hat{\boldsymbol{s}}\\ + \mathscr{R}_5^{\rho}\{\hat{\boldsymbol{p}}\}\mathscr{R}_5^{\rho}\{\hat{\boldsymbol{r}}\}\mathscr{N}_3^{S,s}\{\boldsymbol{q_0}\}\hat{\boldsymbol{s}}\end{aligned} \tag{C 10}$$

$$\mathbb{P}_s^{SS,\epsilon^2}\{\hat{\boldsymbol{p}},\hat{\boldsymbol{r}}\}\hat{\boldsymbol{s}} = \mathscr{R}_{2,3}^{\rho}\{\hat{\boldsymbol{p}}\}\mathscr{N}_2^{SS,s}\{\hat{\boldsymbol{r}}\}\hat{\boldsymbol{s}} \tag{C 11}$$

REFERENCES

Acharya, Vishal, Shreekrishna, Shin, Dong-Hyuk & Lieuwen, Timothy 2012 Swirl effects on harmonically excited, premixed flame kinematics. *Combustion and Flame* **159** (3), 1139 – 1150.

Batchelor, G. K. & Gill, A. E. 1962 Analysis of the stability of axisymmetric jets. *Journal of Fluid Mechanics* **14** (4), 529–551.

Benjamin, T Brooke 1962 Theory of the vortex breakdown phenomenon. *Journal of Fluid Mechanics* **14** (4), 593–629.

Gupta, Saarthak, Shanbhogue, Santosh, Shimura, Masayasu, Ghoniem, Ahmed F. & Hemchandra, Santosh 2021 Impact of a Centrebody On the Unsteady Flow Dynamics of a Swirl Nozzle: Intermittency of PVC Oscillations. *Journal of Engineering for Gas Turbines and Power* **in press**.

Manoharan, Kiran, Frederick, Mark, Clees, Sean, O'Connor, Jacqueline & Hemchandra, Santosh 2020 A weakly nonlinear analysis of the precessing vortex core oscillation in a variable swirl turbulent round jet. *Journal of Fluid Mechanics* **884**.

Mendez, M. A., Balabane, M. & Buchlin, J.-M. 2019 Multi-scale proper orthogonal decomposition of complex fluid flows. *Journal of Fluid Mechanics* **870**, 988–1036.

Moeck, Jonas P, Bourgouin, Jean-François, Durox, Daniel, Schuller, Thierry & Candel, Sébastien 2012 Nonlinear interaction between a precessing vortex core and acoustic oscillations in a turbulent swirling flame. *Combustion and Flame* **159** (8), 2650–2668.

Nayfeh, Ali H 2008 *Perturbation methods*. John Wiley & Sons.

Oberleithner, Kilian, Stöhr, Michael, Im, Seong Ho, Arndt, Christoph M & Steinberg, Adam M 2015 Formation and flame-induced suppression of the precessing vortex core in a swirl combustor: Experiments and linear stability analysis. *Combustion and Flame* **162** (8), 3100–3114.

Tammisola, O. & Juniper, M. P. 2016 Coherent structures in a swirl injector at re = 4800 by nonlinear simulations and linear global modes. *Journal of Fluid Mechanics* **792**, 620–657.

Yin, Zhiyao & Stöhr, Michael 2020 Time–frequency localisation of intermittent dynamics in a bistable turbulent swirl flame. *Journal of Fluid Mechanics* **882**.